# Sparse Registration for Three-Dimensional Stress Echocardiography

K. Y. Esther Leung*, Marijn van Stralen, Attila Nemes, Marco M. Voormolen, Gerard van Burken, Marcel L. Geleijnse, Folkert J. ten Cate, Johan H. C. Reiber, *Fellow, IEEE*, Nico de Jong, *Member, IEEE*, Antonius F. W. van der Steen, *Student Member, IEEE*, and Johan G. Bosch, *Member, IEEE*

***Abstract*—Three-dimensional (3-D) stress echocardiography is a novel technique for diagnosing cardiac dysfunction. It involves evaluating wall motion of the left ventricle, by visually analyzing ultrasound images obtained in rest and in different stages of stress. Since the acquisitions are performed minutes apart, variabilities may exist in the visualized cross-sections. To improve anatomical correspondence between rest and stress, aligning the images is essential. We developed a new intensity-based, sparse registration method to retrieve standard anatomical views from 3-D stress images that were equivalent to the manually selected views in the rest images. Using sparse image planes, the influence of common image artifacts could be reduced. We investigated different similarity measures and different levels of sparsity. The registration was tested using data of 20 patients and quantitatively evaluated based on manually defined anatomical landmarks. Alignment was best using sparse registration with two long-axis and two short-axis views; registration errors were reduced significantly, to the range of interobserver variabilities. In 91% of the cases, the registration result was qualitatively assessed as better than or equal to the manual alignment. In conclusion, sparse registration improves the alignment of rest and stress images, with a performance similar to manual alignment. This is an important step towards objective quantification in 3-D stress echocardiography.**

***Index Terms*—Image registration, stress echocardiography, three-dimensional ultrasound imaging.**

## I. Introduction

### A. Three-Dimensional Stress Echocardiography

CARDIOVASCULAR diseases are a major cause of death in the western world. A commonly used method for detecting myocardial dysfunction and underlying coronary artery disease is stress echocardiography [1]–[5]. This technique is used to evaluate wall motion of the left ventricle (LV), usually by visual examination of ultrasound images that are obtained in rest and in different stages of exercise or pharmacological stress. Recent advances in real-time 3-D echocardiography [6], [7] show great potential in overcoming major limitations of traditional 2-D stress echocardiography, such as variabilities in the visualized LV cross sections and high subjectivity of visual wall-motion scoring. Our long-term goal is to develop more objective and quantitative analysis methods for 3-D stress echocardiography, by automating the image analysis.

We have decided to tackle the automation in three steps: 1) alignment of images acquired in rest and in stress stages, 2) segmentation of the myocardial wall and quantification of wall motion, and 3) automatic classification of wall-motion abnormalities. This paper describes the first step. The alignment of the rest and stress images is necessary because the rest and stress images are acquired several minutes apart, and therefore variations may exist in the visualized cross sections of the LV [8]. Possible sources of misalignment between rest and stress are placement and tilting of the ultrasound probe, as well as patient breathing [9], both of which may lead to inaccuracies when comparing wall motion in the rest and stress stages. We start with image alignment for two reasons. First, registration will greatly assist the segmentation of the myocardial wall by providing a high-quality initialization for the segmentation in the rest image [10]–[12] or the stress image. Second, misalignment will impair the diagnostic quality of the wall-motion differences found in rest and stress, whether by visual scoring or by automatic segmentation. Registration will improve the anatomical correspondence of the LV segments, and will therefore result in a better-quality wall-motion comparison between rest and stress.

### B. Registration Research and Related Work

Intensity-based image registration is widely used for aligning two or more images [13]–[16]. Although most registration work is performed on computed tomography (CT) and magnetic resonance (MR) images, ultrasound image registration has gained considerable interest in recent years [17]. Among the early examples of 3-D ultrasound intensity-based registration are spatial compounding of gall bladder images [18] and registration of breast images [19], [20]. More recent examples include registration of liver images using attribute vectors [21] and tracking brain deformations in intraoperative time series [22]. Registration of ultrasound images with images from other modalities has also been investigated. For example, ultrasound to CT registration was explored by Penney *et al.* for alignment of images

Manuscript received October 25, 2007; revised March 05, 2008. Current version published October 24, 2008. This work was supported in part by the Dutch Technology Foundation STW, in part by the Applied Science Division of The Netherlands Organization for Scientific Research (NWO), and in part by the Technology Program of the Ministry of Economic Affairs. *Asterisk indicates corresponding author.*

*K. Y. E. Leung is with Biomedical Engineering, Cardiology, Thoraxcenter, Erasmus MC, 3000 CA Rotterdam, The Netherlands (e-mail: k.leung@erasmusmc.nl).

M. van Stralen, A. Nemes, M. M. Voormolen, G. van Burken, M. L. Geleijnse, F. J. ten Cate, N. de Jong, A. F. W. van der Steen, and J. G. Bosch are with Biomedical Engineering, Cardiology, Thoraxcenter, Erasmus MC, 3000 CA Rotterdam, The Netherlands.

M. van Stralen, M. M. Voormolen, N. de Jong, and A. F. W. van der Steen are with the ICIN—Interuniversity Cardiology Institute of The Netherlands, 3501 DG Utrecht, The Netherlands.

M. van Stralen and J. H. C. Reiber are with the Division of Image Processing, Radiology, Leiden University Medical Center, 2300 RC Leiden, The Netherlands.

Color versions of one or more of the figures in this paper are available online at http://ieeexplore.ieee.org.

Digital Object Identifier 10.1109/TMI.2008.922685

of the femur and pelvis [23]. Ultrasound to MR registration is mainly used in the context of aligning intraoperative ultrasound images to preoperative MR images of e.g., the liver [24] and the brain [25], [26].

Several papers have been published recently on 2-D and 3-D ultrasound cardiac registration. Using a phase-based similarity measure, Grau *et al.* registered 3-D images acquired from the parasternal and the apical echocardiographic windows [27], [28]. A similar approach was used by Zhang *et al.* to register 3-D cardiac ultrasound images to 2-D MR images [29]. Nonrigid registration with spatial and temporal constraints was used by Ledesma-Carbayo *et al.* to determine cardiac motion in 2-D ultrasound sequences [30], [31]. In the cardiac domain, registration of ultrasound and single photon emission computed tomography (SPECT) images was described by Walimbe *et al.* [32].

Registration of rest and stress images has also been investigated. To study differences in myocardial perfusion between rest and stress, Declerck *et al.* registered SPECT images by aligning myocardial feature points with an adapted iterative closest point algorithm [33]. Delzescaux *et al.* used a surface-based registration algorithm involving geometrical models of the left and right ventricles to align rest and stress MR images [34]. An intensity-based approach using rest and stress templates was proposed by Slomka *et al.* for SPECT images [35]. This method was later augmented with an intensity normalization factor, to account for differences in doses and isotopes used between rest and stress [36]. More recently, Juslin *et al.* studied registration with the mutual information metric to PET images [37]. Independent component analysis was applied to the images before registration to extract the voxels representing cardiac tissues.

Closely related to this study is the work of Shekhar *et al.* on registration of cardiac ultrasound 3-D images, either in the same time sequence [38] or in rest and in stress [9]. Rigid and affine registration using the mutual information similarity measure was investigated. The approach was also used as a first step in cardiac segmentation by Zagrodsky *et al.* [11] and Walimbe *et al.* [12]. However, this full-3-D registration method was evaluated only qualitatively.

### C. Sparse Registration

In this study, a new method was developed to align rest and stress images. The key feature of this method is sparsity: only anatomical four-chamber, two-chamber, and short-axis planes of the rest image are used for the registration. A big advantage of using only sparse image information is that it allows us to define the structures contributing most to correct alignment explicitly. In practice, these anatomical views are usually the starting point for further visual assessment of cardiac motion. Selecting and aligning these rest and stress views consistently are therefore essential steps in wall-motion comparison. An additional advantage of using only sparse views for registration is that the influence of common ultrasound anomalies, such as near-field artifacts and echo reverberations, can be limited. These artifacts can dominate large regions of the image, which distort the calculation of the registration metric. Furthermore, less computation effort is needed than in full-3-D registration.

The focus on sparsity and the quantitative evaluation using a manual gold standard distinguishes this study from the work of Shekhar *et al.* [9], who investigated full-3-D mutual-information registration. Our method bears more resemblance to the slice-to-volume registration as reported by Fei *et al.* [39], rather than to the 3-D to 2-D registration methods where 2-D projections of the 3-D image are registered in 2-D [40].

To reduce the variability in visualized cross sections in 3-D stress echocardiography, an intensity-based, sparse registration method was used to retrieve four-chamber, two-chamber, and short-axis views from 3-D stress images that were equivalent to the manually selected views in the rest images. The focus is on spatial alignment of 3-D rest and stress images, rather than temporal alignment within a single time-sequence. Four similarity measures, the level of sparsity, and optimal resolution levels were investigated. The registration was evaluated quantitatively using 20 end-diastolic and end-systolic patient data sets, with manually annotated points as the gold standard. The registration results were compared with interobserver and intraobserver variabilities in manual alignment. A visual, qualitative assessment of the registration performance was also performed.

## II. Methods

The alignment of rest and stress images was accomplished as follows. First, the anatomical coordinate system, which consists of the major axis (i.e., long axis) of the left ventricle (LV) and the direction of the four-chamber view, was manually defined in the 3-D rest image. Next, the four-chamber (4C), two-chamber (2C), and short-axis (SAX) views were constructed on the basis of this coordinate system. These are standard anatomical views used in echocardiography [41]. Finally, these anatomical views were automatically registered to the 3-D stress image, thus providing the anatomical coordinates in the stress stage. The registration was denoted as sparse, because only the voxels on these anatomical views contributed to the metric calculation. We tested different levels of sparsity by varying the number of SAX planes. The sparse registration was compared with full-3-D registration that used all voxels in the 3-D image.

### A. Manual Selection

For this study, we propose a new method for extracting the anatomical coordinate system from a 3-D image of the left ventricle. The method is reminiscent of cardiac MR image-planning protocols [42] and in agreement with current standards [41]. Recent studies have stressed the importance of selecting nonforeshortened apical views [43], [44], as this is the basis for correct comparison of wall motion. In practice, the clinical expert navigates rather randomly through both rest and stress images at end-diastole, until the anatomical views are sufficiently aligned. Here we present a methodology for consistently annotating key landmarks and deriving consistent views in both rest and stress.

The long axis was determined iteratively. Three points were annotated in an initial vertical, approximately apical long-axis, 2-D plane of the 3-D image: the endocardial apex, which was defined as the highest point in the LV cavity, and two points where the mitral valve leaflets were attached to the mitral valve ring. The new estimate of the long axis was the line through the apex and the center of the two mitral valve points. Next, the plane

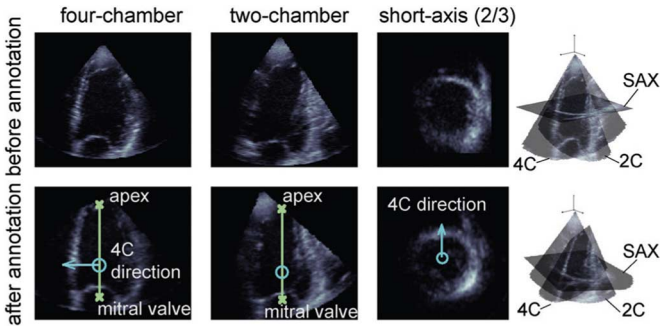


Fig. 1. Orthogonal four-chamber (4C), two-chamber (2C), and short-axis (SAX) views of an ED image. The right column shows the orientation of the orthogonal planes in 3-D space.

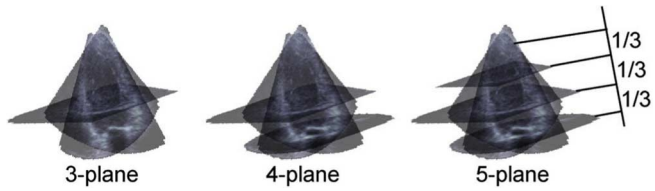


Fig. 2. Registration using different levels of sparsity: configurations with four-chamber, two-chamber, and varying number of short-axis planes.

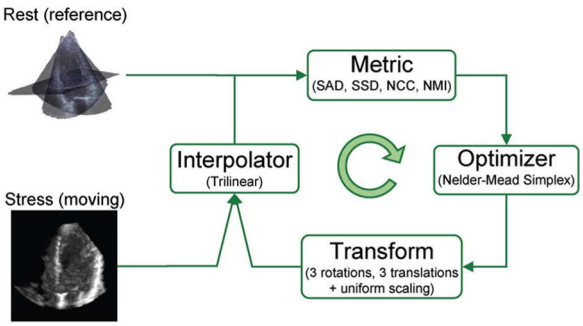


Fig. 3. Schematic of registration framework. The sparse rest image is registered to the stress image in 3-D.

perpendicular to the initial vertical plane and coinciding with the long axis was reconstructed. The annotation and the plane reconstruction were repeated, until the long axis was correct in both perpendicular planes. By annotating the points iteratively, the indicated points converged in the true positions. In practice, this takes only three to four iterations and is quite fast to perform.

The 4C direction was determined by examining several candidate long-axis planes 4° apart, 50° counter-clockwise from the aorta outflow tract, which was indicated manually on the short-axis plane at the height of the mitral valve center. This 50° angle was an initial guess, the observer could correct the angle manually afterwards by indicating the desired direction in the short-axis plane. The 4C plane was defined as transecting the long axis and the centre of the tricuspid valve. As an additional anatomical landmark for evaluating registration, the posterior attachment of the right ventricular wall, RV-attachment for short, was also annotated. This was indicated in the short-axis plane between the mid and basal section of the LV, at two-thirds of the apex-to-mitral-valve distance.

The 2C view was defined as orthogonal to the 4C plane and also passing through the long axis. Short-axis planes orthogonal to 4C and 2C were defined at different points along the long axis. An example of manual annotation is given in Fig. 1, showing the large difference in spatial location between the sparse planes and the original, unselected views.

### *B. Rest to Stress Registration*

The anatomical views of the rest image were registered to the 3-D stress image using a similarity transform. We investigated sparse image registration using different configurations of planes. The three-plane configuration consisted of the 4C, 2C, and one basal short-axis plane at two-thirds of the apex-to-mitral-valve distance. The four-plane configuration consisted of three-plane plus an additional short-axis plane at the mitral valve height. The five-plane configuration is four-plane plus the apical short-axis plane at one-third of the apex-to-mitral-valve distance. These configurations are shown in Fig. 2.

Although nonrigid registration is often applied to achieve very precise image alignment, a relatively simple similarity transform was used in this study. The most important reason for this choice was that we intended to compensate global misalignment of the anatomical coordinates in the rest and stress images, and not local, stress induced, misalignment of all LV wall segments. In a later stage, nonrigid registration might be applied to examine local wall-motion abnormalities more precisely [30]. Furthermore, nonrigid registration usually needs a good initialization, which can be provided by rigid registration [45]. In addition, nonrigid registration is generally very slow and computationally intensive. To limit any nonrigid motion which may be caused by breathing [46], the images were acquired during one breathhold, after full exhalation.

The main components of registration are the optimizer, the transform, the interpolator, and the similarity metric. A schematic representation is given in Fig. 3. In this study, the transform consisted of $(x, y, z)$ rotation, $(x, y, z)$ translation, and uniform scaling. Rotation and translation were needed to compensate for 1) patient breathing, which causes displacement of the heart within the thorax; 2) differences in placement of the probe on the patient's body, and 3) for differences in the probe's tilt angle which were often needed to capture the whole LV in the image optimally. Uniform scaling was intended to account for the possible volume differences between rest and stress [9].

The parameters of the transform were optimized using the Nelder-Mead downhill Simplex algorithm [47]. This optimizer has been used in other registration problems as well [9], [20], [35], [38], [39]. The method involves constructing an enclosing shape, or simplex, in the $N$-dimensional parameter space from $(N + 1)$ vertexes. In a 2-D parameter space, this would be a triangle, in 3-D a tetrahedron, etc. In our 7-D parameter space these eight vertexes represent combinations of the rotation, translation and scaling parameters. During optimization, the metric is calculated at all vertexes of the simplex and the vertexes are reflected, expanded, or contracted accordingly, until the simplex is small enough and has therefore converged to a solution [48]. This optimization method distinguishes itself from gradient-based techniques that are more sensitive to local

minima in the parameter space. Local minima may often occur in the case of ultrasound images, due to the highly anisotropic image formation and speckle noise [49]. The simplex method does not require computation of partial derivatives and may therefore be more robust in a complicated parameter space. Other advantages are that it is easy to implement and provides a good compromise between robustness and convergence time [49].

Normalized parameters were used during optimization in simplex space. One unit simplex parameter corresponded to 1.1 mm translation, 0.4° $(x, y)$ rotation, 0.5° $z$ rotation, and 0.7% scaling. The parameters' normalization factors were determined on the basis of the physical displacement of the image voxel furthest away from the origin of the transform. As an example, an $x$ rotation of 0.4° performed on the voxel furthest away from the rotation origin, i.e., in the lowest corner of the image, will lead to a physical displacement of 1.1 mm (calculated on a typical data set of $160 \times 144 \times 208$ voxels of 1.1 mm $\times$ 1.1 mm $\times$ 0.7 mm). To correct for the tilt angle of the ultrasound probe easily, the centre of the transducer was chosen as the origin of rotation. To preserve the position of the LV as much as possible, the origin of scaling coincided with the centre of the image. The initial size of the simplex was 3 units along each parameter axis. Registration was considered to be converged when the simplex hypervolume was smaller than 0.01 and when the differences in metric value at the simplex vertexes were less than $10^{-4}$. Trilinear interpolation was used because of computational efficiency.

In our sparse registration setup, we tested several similarity metrics which are commonly used in registration [13], [16], [50]: sum-of-absolute-differences (SAD), sum-of-squared-differences (SSD), normalized cross correlation (NCC), and normalized mutual information (NMI). NMI was calculated with the histogram method [51]. A bin size of 2 was used for the 8-bit data; this was found empirically. Voxels outside the transducer's scan sector did not contribute to the metric calculation. Registration was carried out on four separate resolution levels of a Gaussian image pyramid [52]; from full resolution at level 0 to 8 times downsampled at level 3. A multiresolution scheme was also tested.

The sparse image grid was initialized in the stress image, at the same spatial coordinates as the rest image. At each registration iteration, the spatial transform was applied to the coordinates of the sparse rest-image grid. The stress image was then resampled at those coordinates using trilinear interpolation. The metric was calculated using only the voxels on the sparse grid. In this manner, anomalies such as near-field artifacts and echo reverberations, which may dominate the metric calculation, could be avoided as much as possible.

### C. Data Description and Algorithm Evaluation

Full-cycle 3-D data sets were acquired at the Thoraxcenter (Erasmus MC, Rotterdam, The Netherlands) on 20 patients in sinus rhythm with chest pain referred for stress testing. A Dobutamine-Atropine stress protocol was used [53]. All data sets were obtained in the apical position; each image sequence was obtained during one breathhold. Patients were imaged at rest and at peak-dose. The data sets for three patients were acquired with the Fast Rotating Ultrasound transducer [54] developed at the department of Biomedical Engineering (Thoraxcenter, Erasmus MC, Rotterdam, The Netherlands). The spatial dimension of the images were $128 \times 128 \times 388$, at 1.4 mm $\times$ 1.4 $\times$ 0.3 mm (length $\times$ width $\times$ depth). The remaining 17 patients were examined using the commercially available Philips Sonos 7500 machine equipped with the X4 matrix-array transducer (both from Philips Medical Systems, Andover, MA). These images contained $160 \times 144 \times 208$ voxels of 1.1 mm $\times$ 1.1 mm $\times$ 0.7 mm. Registration was tested on 3-D rest-and-stress image pairs at end-diastole (ED) and end-systole (ES) separately, because the left ventricle may move differently under stress conditions. We chose to evaluate the registration on ED and ES time points because these could be clearly identified for each sequence. ED and ES time points were defined, respectively, by the ECG R-peak and by the mitral valve opening.

To get an overall idea of image quality, the visibility of the 17 LV wall segments [41] was judged visually by an expert observer, blinded from the registration results. Each segment was given a score: $4 =$ optimal, $3 =$ good, $2 =$ moderate, $1 =$ poor, $0 =$ invisible [53]. This was done for all rest and stress image sequences. The average of the 17 scores was then calculated for each patient.

Interobserver and intraobserver variabilities were also analyzed. Two independent observers indicated the long axis and 4C direction, as well as the aorta, and the RV-attachment in end-diastole and end-systole. The first observer annotated each data set twice, at an interval of at least one day. The second observer indicated 11 rest and 11 stress data sets twice, and the remaining data sets once. The intraobserver variability in the apex, mitral valve centre, aorta and RV positions was defined as the average of Euclidean distances between annotated points. The intraobserver variability in the 4C angle was defined as the average of absolute differences in angle. Mean and standard deviations were calculated over all indicated data sets. The interobserver variability was defined similarly, as the average of differences in the mean annotation of each observer.

Since we were interested in aligning only the anatomical views, a natural choice of landmarks for quantitative evaluation of the registration were the landmarks on the sparse planes. The following landmarks were chosen because they were adequately salient structures in the images: the apex and mitral valve points, the direction of the four-chamber, the aorta outflow tract, and the posterior attachment of the right ventricular wall. Although only these landmarks were evaluated, the rest-to-stress point correspondence of the whole myocardial border should also benefit from a good initial alignment. Further comparison of 3-D wall-motion might be hampered if the global anatomical coordinate system was not well defined.

The average over all annotations (three to four per data set) was used as the anatomical coordinate system for the registration, thus providing a gold standard. The registration errors for each image-pair were defined as the point-to-point Euclidean distances between the gold standard and the registered landmarks. The initial error was defined as the point-to-point distances between the gold standard and the initial position of the

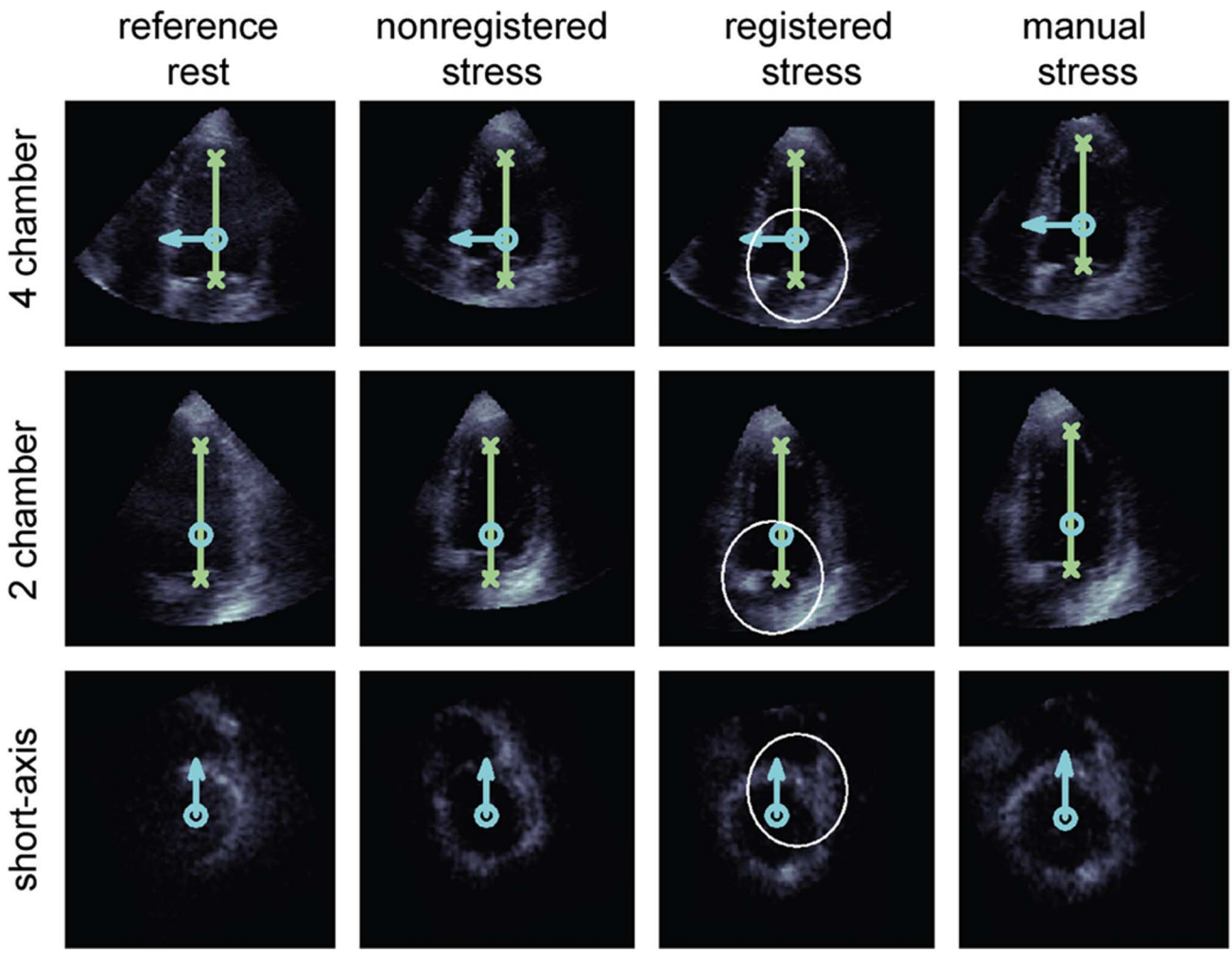


Fig. 4. Orthogonal four-chamber, two-chamber, and short-axis views. Before registration, the anatomical landmarks are misaligned in the stress images. The results of registration are in good agreement with manual annotation. The circles indicate improvement in alignment.

landmarks (the same spatial coordinates as the manual annotation in the rest image). The errors were calculated for each anatomical landmark and for each rest-stress image pair separately. The registration error was then compared with the initial error using the paired $t$-test [55]. The registration errors were also compared with the interobserver and intraobserver variabilities in manual annotation.

In addition to the quantitative evaluation, a qualitative assessment was performed by an independent observer, blinded from the registration results. The observer was presented four-chamber, two-chamber, and short-axis views of 1) the manually annotated rest image, 2) the manually annotated stress image, 3) the stress image before alignment (initialized by the landmarks indicated in the rest image), and 4) the stress image after registration, similar to Fig. 4. The observer did not know whether set 3) or set 4) corresponded with images before or after registration. First of all, to determine whether the registration resulted in better rest-to-stress alignment, the observer judged if set 3) or 4) was better aligned with set 1), or if there was no visible difference, or if visual assessment was impossible due to poor image quality. A set was considered better aligned if the position of the long-axis and the direction of the four-chamber view in the stress image showed a better correspondence with the rest image. Second, the observer judged whether the set that was selected in the first part of the experiment was worse, equally, or better aligned with the rest image than the *manually indicated* stress image, again on the basis of the long-axis position and four-chamber view.

## III. Results

### A. Annotation of Landmarks

Two independent observers indicated the apex, the mitral valve, the RV-attachment on the short-axis view of the three-plane configuration, the aorta center in the short-axis view at mitral-valve height, and the four-chamber direction. Typically, four three-point annotations were needed to indicate the long-axis correctly in both perpendicular long-axis views. The annotation was carried out in Matlab [56], which took a few minutes per dataset. Later, we developed dedicated visualization software in C++. Using this program, the annotation time was reduced to less than half a minute for each 3-D image. The interobserver and intraobserver variabilities are shown in Table I. Of the five landmarks, the mitral valve was the easiest to annotate, because it was usually a clear salient structure in the image.

TABLE I
EFFECT OF USING DIFFERENT REGISTRATION SPARSITY. REGISTRATION ERRORS IN FIVE ANATOMICAL LANDMARKS USING NCC METRIC AND FULL-RESOLUTION DATA. INTEROBSERVER AND INTRAOBSERVER VARIABILITIES ARE ALSO GIVEN. $*$ MEANS STATISTICALLY SIGNIFICANTLY LOWER ERROR THAN BEFORE REGISTRATION ($p < 0.05$, PAIRED $t$-TEST)

| Sparsity | Apex mm | Mitral valve mm | 4C ° | RV mm | Aorta mm |
|---|---|---|---|---|---|
| Median [25% 75% percentiles] | | | | | |
| Error before registration | 9.3 [5.3 13.2] | 8.3 [6.1 11.3] | 8.9 [5.0 14.7] | 9.7 [7.6 14.4] | 10.2 [7.0 13.9] |
| Interobserver variability | 6.3 [4.7 9.4] | 3.5 [3.1 4.6] | 6.6 [4.8 10.7] | 4.7 [3.8 6.4] | 6.1 [4.3 9.1] |
| Intraobserver variability | 4.5 [3.3 6.1] | 2.9 [2.3 3.6] | 5.8 [3.4 8.1] | 5.0 [3.3 6.4] | 5.1 [3.9 8.0] |
| 3-plane | 6.1 [3.9 9.7] | 4.5 [2.4 7.5] | 7.3 [5.0 10.4] | 5.8 [3.2 7.8] | 6.5 [3.9 10.8] |
| 4-plane | 7.0 [4.0 9.4] | 3.6 [2.3 6.0] | 7.1 [4.8 10.7] | 5.2 [3.8 8.0] | 6.7 [4.5 9.1] |
| 5-plane | 6.2 [4.3 10.0] | 4.4 [2.3 7.1] | 6.2 [3.7 10.3] | 4.8 [3.0 9.3] | 7.0 [4.1 10.6] |
| full-3-D | 9.7 [4.3 17.1] | 5.6 [2.7 9.3] | 6.5 [3.1 10.7] | 6.5 [3.6 10.8] | 8.4 [4.7 15.5] |
| Mean $\pm$ standard deviation | | | | | |
| Error before registration | 9.4 $\pm$ 5.1 | 9.0 $\pm$ 4.0 | 9.9 $\pm$ 5.6 | 10.9 $\pm$ 5.5 | 11.0 $\pm$ 5.9 |
| Interobserver variability | 7.1 $\pm$ 2.9 | 3.8 $\pm$ 1.3 | 7.4 $\pm$ 4.0 | 5.0 $\pm$ 1.8 | 6.8 $\pm$ 4.2 |
| Intraobserver variability | 5.2 $\pm$ 2.0 | 3.3 $\pm$ 1.5 | 7.0 $\pm$ 3.5 | 5.5 $\pm$ 2.1 | 6.9 $\pm$ 3.2 |
| 3-plane | 7.7 $\pm$ 4.9* | 5.7 $\pm$ 4.9* | 8.4 $\pm$ 4.8 | 6.6 $\pm$ 5.1* | 7.8 $\pm$ 5.7* |
| 4-plane | 7.6 $\pm$ 4.8* | 4.5 $\pm$ 2.9* | 7.8 $\pm$ 4.3* | 6.3 $\pm$ 4.6* | 7.6 $\pm$ 5.4* |
| 5-plane | 7.6 $\pm$ 5.4* | 5.4 $\pm$ 4.4* | 7.2 $\pm$ 4.6* | 6.5 $\pm$ 5.2* | 7.8 $\pm$ 5.7* |
| full-3-D | 11.8 $\pm$ 9.2 | 8.9 $\pm$ 14 | 8.3 $\pm$ 6.7 | 9.4 $\pm$ 9.5 | 12 $\pm$ 14 |

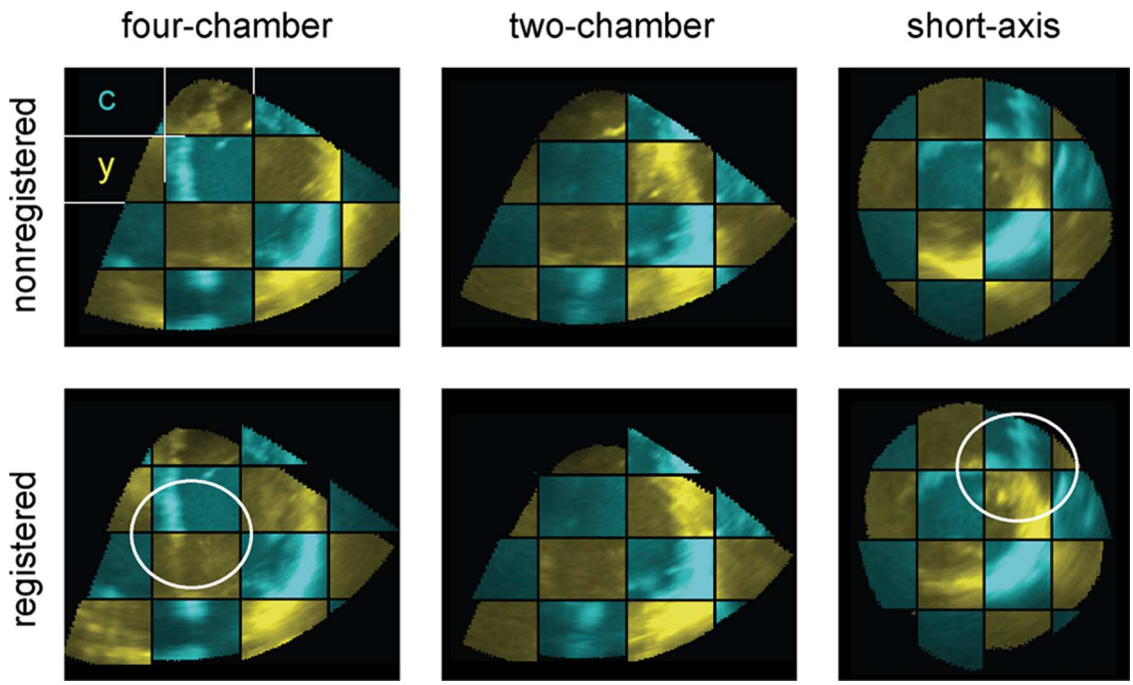


Fig. 5. Checkerboard images of rest (cyan (c); top left patch in all images) and stress (yellow (y)). Alignment improvement is clearly visible after registration, especially in the four-chamber view and in the short-axis view. The circles indicate improvement in alignment.

### B. Image Quality Assessment

Using the image-quality scoring system described in the methods section, we found that the overall image quality was moderate, with a mean score of $2.0 \pm 1.0$ on a scale of 0 (invisible) to 4 (optimal), averaged over the 20 rest and 20 stress time-sequences. The maximum score was 4, the minimum score was 0.46, and the median was 1.85. Not only the image quality itself, but also the difference in image quality between rest and stress could compromise the registration. The absolute difference between rest and stress, averaged over the 20 patients, was $0.82 \pm 0.70$, the maximum score was 2.1, the minimum was 0, and the median was 0.76. This shows the large difference in image quality between rest and stress. The image quality in the rest images was generally better than in the stress images (16 out of 20 patients).

### C. Qualitative Assessment of Registration

Fig. 4 shows an example of registration using a Philips data set. The set of orthogonal four-chamber, two-chamber, and short-axis views of the rest image is shown, along with the nonregistered, registered, and manually selected views of the stress image. The registered views correspond well with the manual selection. An example of the results using a FRU data set is presented in Fig. 5. There did not seem to be any

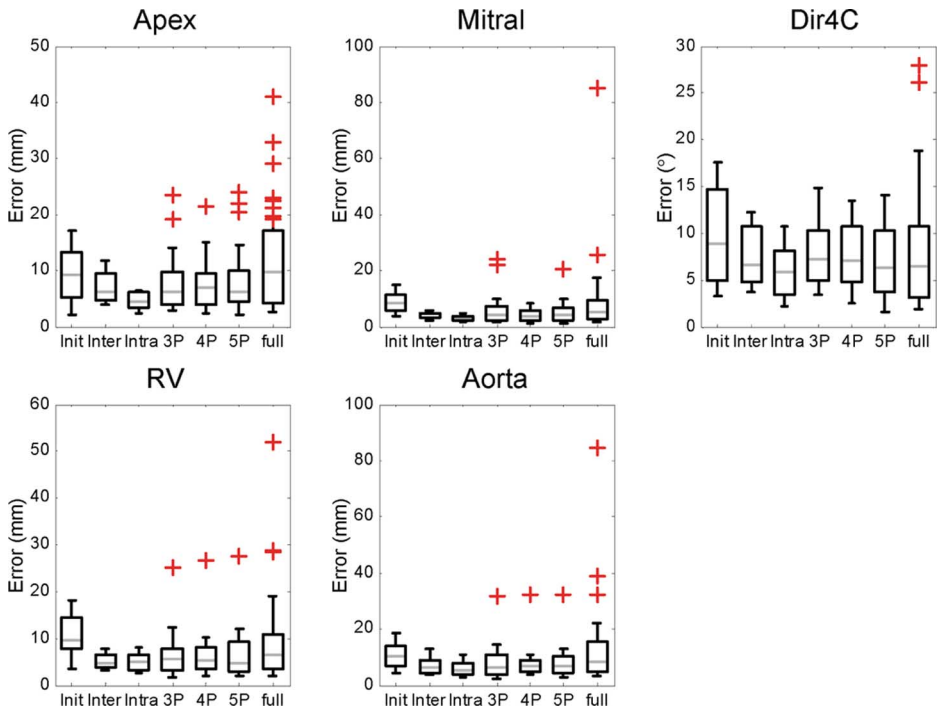


Fig. 6. Registration errors in five landmarks, using different levels of sparsity. The boxes indicate the 25%, 50% and 75% percentiles; the whiskers represent 10% and 90% percentiles. Outliers are shown as red plus signs. Registration using the four-plane configuration appears most robust.

TABLE II
QUALITATIVE ASSESSMENT OF SPARSE REGISTRATION (SPARSE FOUR-PLANE CONFIGURATION, NCC METRIC, FULL-RESOLUTION DATA), 20 ED AND 20 ES IMAGES

| | Better than manual annotation in stress | Same as manual annotation in stress | Worse than manual annotation in stress | Total |
|---|---|---|---|---|
| Registered better than nonregistered | 7 | 19 | 3 | 29 |
| Registered equal to nonregistered | 0 | 4 | 0 | 4 |
| Registered worse than nonregistered | 0 | 2 | 0 | 2 |
| Poor image quality | 0 | 5 | 0 | 5 |
| Total | 7 | 30 | 3 | 40 |

noticeable differences in registration accuracy between the FRU and the Philips data sets; however, since only 3 FRU data sets are available, no clear conclusion can be drawn.

The registration using the four-plane configuration, the NCC metric, and full resolution images resulted in the lowest mean registration errors. Therefore, these registrations were assessed qualitatively by the independent observer, in all 20 ED and 20 ES image pairs. The results are shown in Table II. In the majority of the cases (29/40) the observer selected the registered stress image as the image best aligned with the rest image, while in 9 out of 40 cases the registered image was either equal to the nonregistered image or could not be judged because of poor image quality. Remarkably, in 30 out of the 33 cases (91%) where the registered image was better than or equal to the nonregistered image, the registration was better than or equal to the manual annotation.

### D. Quantitative Assessment of Registration

*1) Sparsity:* Fig. 6 and Table I show the results of registration using the normalized cross-correlation metric and full-resolution data for different levels of sparsity. The registration errors over 20 ED and 20 ES image-pairs are presented for each of the five landmarks. Minimal differences in errors were found between ED and ES image-pairs. Lower median errors were found in most cases, for both sparse and full-3-D registration. The 25%–75% percentile range of registration errors is quite close to the interobserver range (Fig. 6). In particular, the mean errors of the sparse registration with the four-plane configuration were the lowest, and comparable with the interobserver variability (Table I). A closer inspection revealed that the mean errors of full-3-D were distorted because of outliers of some image pairs (Fig. 6). For each landmark, the registration of a rest-stress image pair was considered failed if the registration error was higher than the maximum initial error encountered in all 20 ED and 20 ES image pairs. These maximum initial errors were 18.6 mm for the apex, 20.4 mm for the mitral valve, 22.8° for the four-chamber direction, 24.6 mm for the RV-attachment, and 30.4 mm for the aorta.

Although the differences between the different levels of sparsity were small, registration using the four-plane configuration appeared to be most robust (Fig. 6). Therefore, we will show registration results using this four-plane configuration in the following.

*2) Registration Metric:* Table III shows the results of registration with the four-plane configuration, for the SAD, SSD,

TABLE III
EFFECT OF USING DIFFERENT REGISTRATION METRICS. REGISTRATION ERRORS IN FIVE ANATOMICAL LANDMARKS USING FOUR-PLANE CONFIGURATION AND FULL RESOLUTION DATA. INTEROBSERVER AND INTRAOBSERVER VARIABILITIES ARE ALSO GIVEN. MEAN ± STANDARD DEVIATION OF REGISTRATION ERRORS. ∗ MEANS STATISTICALLY SIGNIFICANTLY LOWER ERROR THAN BEFORE REGISTRATION ($p < 0.05$, PAIRED $t$-TEST)

| Metric | Apex mm | Mitral valve mm | 4C ° | RV mm | Aorta mm |
|---|---|---|---|---|---|
| Error before registration | 9.4±5.1 | 9.0±4.0 | 9.9±5.6 | 10.9±5.5 | 11.0±5.9 |
| Interobserver variability | 7.1±2.9 | 3.8±1.3 | 7.4±4.0 | 5.0±1.8 | 6.8±4.2 |
| Intraobserver variability | 5.2±2.0 | 3.3±1.5 | 7.0±3.5 | 5.5±2.1 | 6.9±3.2 |
| SAD | 9.1±5.7 | 5.3±3.0* | 7.8±5.3* | 7.3±5.0* | 8.2±5.7 |
| SSD | 9.8±5.9 | 5.7±6.2* | 8.4±5.1 | 7.9±6.7* | 8.7±8.3 |
| NCC | 7.6±4.8* | 4.5±2.9* | 7.8±4.3* | 6.3±4.6* | 7.6±5.4 |
| NMI | 9.0±5.6 | 6.1±3.7* | 7.6±5.1* | 7.4±4.9* | 8.6±6.3 |

TABLE IV
EFFECT OF USING IMAGE DATA AT DIFFERENT RESOLUTIONS, FROM FULL RESOLUTION (0) TO EIGHT TIMES (3) DOWNSAMPLED DATA, AS WELL AS MULTIRESOLUTION (1-0). REGISTRATION ERRORS IN FIVE ANATOMICAL LANDMARKS USING THE NCC METRIC AND FOUR-PLANE CONFIGURATION. ∗ MEANAS STATISTICALLY SIGNIFICANTLY LOWER ERROR THAN BEFORE REGISTRATION ($p < 0.05$, PAIRED $t$-TEST). STATISTICAL TESTING WAS NOT PERFORMED AFTER OUTLIER REMOVAL

| Resolution | Apex mm | Mitral valve mm | 4C ° | RV mm | Aorta mm |
|---|---|---|---|---|---|
| 0 | 7.6±4.8* | 4.5±2.9* | 7.8±4.3* | 6.3±4.6* | 7.6±5.4* |
| 1 | 8.8±5.6 | 4.8±4.2* | 8.9±6.5 | 6.9±5.2* | 8.8±7.9 |
| 2 | 9.5±6.1 | 5.5±3.9* | 8.6±7.1 | 6.9±5.0* | 9.1±8.0 |
| 3 | 11.7±6.1 | 6.7±4.7* | 9.5±6.8 | 8.2±5.8* | 9.5±6.7 |
| After outlier removal | | | | | |
| 1-0 | 7.7±4.1 | 4.3±3.0 | 7.5±4.3 | 5.6±3.3 | 6.8±4.5 |
| 0 | 7.1±3.9 | 4.2±2.4 | 7.4±3.8 | 5.6±3.2 | 6.8±3.7 |
| 1 | 8.1±4.1 | 4.4±2.8 | 7.8±4.1 | 5.7±3.4 | 7.2±4.2 |

NCC, and NMI metrics. Registration using the NCC metric improved the alignment in all five landmarks statistically significantly.

*3) Image Resolution:* Table IV shows the registration results for different image resolutions. Registration on full resolution data performed better than registration on downsampled data. We also tested a multiresolution scheme, starting at resolution level 1, and finishing at level 0. In 4 out of 40 cases, the registration in level 1 resulted in an outlier for at least one landmark. In those cases, further registration on level 0 resulted in minimal improvement. Therefore, these cases were not taken into account in the reported multilevel results. In this subset of registration image pairs, minimal differences in results were found between the multilevel approach and the single level 0 approach.

*4) Registration Time:* The registration time was calculated for the NCC metric, for different resolution levels and for the different levels of sparsity. This is reported in Table V. The times were calculated using a Matlab implementation [56] and a 2.8-GHz Intel Pentium 4 processor. The implementation was not optimized for speed. The sparse registration using four-plane configuration at resolution level 1 is on average thirteen times faster than full-3-D registration. Due to memory limitations, the full-3-D registration at resolution level 0 had to be implemented differently, and those times are not reported here. The multilevel method using the four-plane configuration took on average $12 \pm 6$ min per registration.

TABLE V
MEAN ± STANDARD DEVIATION OF REGISTRATION TIMES (MIN), NCC METRIC

| Sparsity | Resolution level 0 | 1 | 2 | 3 |
|---|---|---|---|---|
| 3-plane | 13±8 | 2.5±2.8 | 0.45±0.17 | 0.15±0.07 |
| 4-plane | 21±14 | 3.0±1.9 | 0.54±0.22 | 0.17±0.05 |
| 5-plane | 23±16 | 3.5±2.4 | 0.61±0.31 | 0.18±0.05 |
| full-3-D | - | 41±23 | 4.3±1.7 | 0.43±0.17 |

## IV. DISCUSSION

This study shows that the variability in visualized cross sections in 3-D stress echocardiography can be reduced by using sparse image registration. Registration leads to visually better-aligned rest and stress images, in some cases better than the manual alignment. The quantitative registration errors were comparable with the interobserver variabilities in the manual selection of the anatomical coordinates. Given the moderate image quality and the large differences in appearance between rest and stress images, this is a promising result.

### A. Annotation of Landmarks and Image Quality

The annotation of landmarks was a fairly easy task which required little user interaction. Typically, three to four iterations (9–12 mouse clicks) were required to locate the long-axis, with additional one or two clicks to identify the four-chamber direction. The overall image quality was comparable to that found in a larger study with 36 consecutive patients referred for stress echocardiography (image quality score: 2.0 in this study, versus 2.2 in [53], scored by the same observer in both studies). Although the annotation protocol was fixed and should lead to consistent results, in some cases, the precise location of the landmarks were unclear due to poor image quality. This is reflected in the rather large interobserver and intraobserver variabilities (Table I). Moderate image quality remains a great challenge in the clinical practice of echocardiography, especially in 3-D [57]. In the near future, significant improvements can be expected in ultrasound imaging technology, and these improvements will also positively affect image analysis. Although the definition of the gold standard was hampered by the limited image quality, we can still draw some conclusions on the effectiveness of sparse registration based on average values over all data sets.

### B. Qualitative Assessment

Qualitative assessment of the registration paints a positive picture: in the majority of the cases, sparse registration was able to achieve equally good rest-to-stress alignment. More importantly, in several cases, the alignment was considered even better than the manually aligned data sets. Since the rest and stress images were not manually annotated next to each other, differences could occur between the landmark annotation and the actual landmark position. This is especially the case for landmarks which were difficult to define because of poor image quality. This may explain why the registered stress image was considered better in terms of landmark placement in 7/40 cases.

### C. Sparse Registration

The poor image quality affected the definition of the gold standard, which in turn may have influenced the determination of registration success. We showed that the registration error was comparable to the interobserver variabilities of several key landmarks. However, due to the definition of the gold standard, results may not seem outstanding compared to subvoxel precision reported in some papers. However, the qualitative assessment suggests that the registration method is actually quite good, and that rest-to-stress alignment can be achieved in most cases. The sparse registration method is qualitatively assessed as comparable to manual alignment, and will therefore benefit the analysis of rest and stress.

Since we were interested in alignment of the anatomical views, we chose salient landmarks on these sparse planes for evaluating both sparse and full-3-D registration. For an accurate comparison between rest and stress, it is important to first achieve global image alignment before more detailed registration. From this study, we can conclude that for initialization purposes, sparse registration is a better and a more robust choice than full 3-D registration of echocardiographic images. Naturally, since sparse registration does not take into account areas of the left ventricle outside the sparse planes, no conclusions can be drawn with respect to alignment in those areas. However, the nonrigid, full-3-D registration of the whole left ventricle requires a good, robust initialization, which can be achieved using sparse registration. Ultrasound images tend to contain many anomalies, such as near-field artifacts, echo dropouts, and acoustic shadowing and noise, all of which can easily mislead full-3-D registration. In fact, one of the advantages of using a sparse approach is to avoid such artifacts, as mentioned in the introduction. Ultrasound artifact suppression is neither trivial nor easy to do. A robust, automated method for detecting such artifacts warrants further study.

Our results demonstrated that when sparsity changes from the three-plane to the four-plane configuration, better alignment is achieved in all manually annotated landmarks. Similar results have been shown in sparsity experiments for other applications. Using a sparse active shape model for segmenting cardiac MR images, Van Assen *et al.* [58] showed that a higher number of short-axis planes reduced segmentation errors. However, no significant improvement was found using six planes or more. In a slightly different application, Pang showed that accurate volumetric measurements of phantoms with complex geometries could be achieved using a limited number of ultrasound image planes [59]. These findings are in good agreement with the results reported by Voormolen *et al.* in an *in vivo* cardiac setting [60]. These reports show that only eight planes in 3-D images are sufficient for adequate volume analysis. In our case, using the five-plane instead of four-plane configuration had a negative effect on the alignment in the mitral valve region. This may be a consequence of adding an extra short-axis plane in the apical region, thus reducing the relative contribution of the mitral plane to the metric calculation. However, a slight improvement can be seen in the alignment of the four-chamber direction, probably because a small part of the right ventricular wall can be seen in the extra short-axis plane at the apical level. The fact that the results are very close to the interobserver variabilities suggests that a better gold standard is needed to determine whether other configurations of planes lead to better results. This is a subject of further investigation.

Better alignment was achieved in the mitral valve region than in the apical region. Several factors may have contributed to this. First of all, the apex is quite often obscured by near-field artifacts or is partly outside the scan sector, while on the other hand, the mitral valve region usually contains more structural information such as the aortic and tricuspid valve, which helps alignment in the four-chamber direction. Second, due to our choice of image planes, the number of voxels contributing to the metric calculation was higher at the mitral valve region. In an earlier registration experiment, we tried to register only the apex, using just the top third of the long-axis planes and one short-axis plane in the apical region. However, the near-field artifacts caused misalignment in a considerable number of cases. We expect that suppressing these stationary signals will lead to better alignment in the apical area, for example using harmonic imaging techniques [61].

### D. Registration Metric

The best results were obtained using the NCC metric. Whereas SSD implicitly assume that images differ only in terms of Gaussian noise, the NCC makes a less strict assumption of linear relationship between the intensity values [13], [16]. This assumption is more valid in our case, because ultrasonic image formation is highly anisotropic and position-dependent across the different rest and stress acquisitions. Global brightness variations caused by differences in gain settings may exist between the rest and stress images, which can be more adequately handled with normalized metrics [50].

SAD performed slightly better than SSD in our study, probably because SAD is less sensitive to outliers [13]. This is in accordance with the results reported by Cohen and Dinstein [62], and in the closely related field of speckle tracking in ultrasound images [63], [64]. Although SAD performed better than SSD in our study, it cannot be interpreted as a general finding. The choice for metrics remains very much modality and application dependent.

NMI on the other hand performed slightly worse, probably because the number of voxels in the sparse planes was not large enough for computing the joint histogram reliably [15]. Otte reached the same conclusion when comparing NCC with NMI in registering subsets of functional MR images [65]. One solution to this problem may be to combine the probability distribution of the whole image with the local distribution of the sparse planes, as proposed by Likar and Pernuš [66].

Sophisticated metrics that are specially designed to deal with the complicated noise distribution in ultrasound data, may lead to small improvements in registration accuracy. For example, Cohen and Dinstein proposed new maximum likelihood metrics for ultrasound images, contaminated by Rayleigh distributed multiplicative noise [62]. Their results on simulated and *in vivo* images showed that the new metrics outperformed SAD and SSD. In our images, however, we suspect that the influence of the acquisition-related artifacts (echo dropouts, acoustic shadowing) is stronger than speckle-related artifacts. Phase-based

measures may therefore be a more suitable alternative, and their effectiveness has been demonstrated in registering global structures in ultrasound images [28]. However, this is beyond the scope of our study.

### *E. Image Resolution*

Registration was best at finer resolutions, despite the Gaussian filtering in coarser resolution levels. Although Gaussian filtering can remove speckle noise, it may also blur the edges of the myocardial wall, resulting in lower registration accuracy. Also, at the coarser resolutions, most of the salient structures had disappeared due to filtering. Anisotropic filtering should be able to preserve these structures while removing speckle noise [67]. Furthermore, since only sparse image planes were used in the registration, it is more important to preserve the amount of information in the sparse planes. This also explains the slightly better results of the single level registration at full resolution than those of the multilevel registration. In particular, in the apical region, downsampling might have removed too much image information, as can be seen in the registration errors (Table IV). In the case of such sparse planes, it is best to always use the full resolution data which contains the full image information. The multilevel registration did not seem to contribute to more robust results, probably because the initialization of the landmarks was already pretty close to the optimum.

### *F. Limitations and Comparison With Other Work*

Although the list of possible configurations of sparse planes is unlimited, we have demonstrated that adequate results could be achieved by using very sparse images.

Because our study aim was to achieve global alignment of rest and stress images, rigid registration was used. Nonrigid registration, however, should give a more exact alignment of the different myocardial wall segments, although it is much slower [13]. It might also be used for comparing wall motion between rest and stress stages. This should be investigated in future research. Other issues in the registration framework which can be further investigated are the type of optimizer, such as simulated annealing. Although slower in convergence, it may be more robust and can also be implemented within the simplex framework [48], [49]. For NMI, partial volume interpolation should help make the metric function smoother [51].

Shekhar *et al.* [9] reported achieving visually better aligned images using full-3-D mutual-information registration. Full-3-D registration did not give the best results in our experiments; however, we cannot compare their results with ours directly. First, their results on rest-to-stress registration were evaluated only visually and their work did not relate to sparsity. Second, their images were acquired using the Volumetrics scanner (Durham, NC) and ours mainly using the Philips Sonos 7500 system (Philips Medical Systems, Andover, MA). Furthermore, the stress was induced physically using a supine bicycle in their case, whereas a dobutamine protocol was used in this study. Regarding their similarity measure, the mutual-information metric was calculated on median filtered data, using partial-volume interpolation, which should be more robust. However, we believe that application of our sparse method would be beneficial in the approach of Shekhar *et al.* [9], provided a suitable algorithm for calculating the joint histogram on sparse planes is used. This is a subject of further investigation.

To fully analyze the differences in left-ventricular wall motion between rest and stress, a full 3-D examination of the alignment outside the sparse image planes is necessary. Since the goal of this study was to globally align the anatomical coordinate system in both images, the registration was evaluated using only salient landmarks within the sparse planes. One way of examining the alignment outside these planes might be to compare manual segmentations of the 3-D endocardial surface in the rest and stress sequences, provided that these can be drawn accurately. Since the images are globally aligned, the distances between the 3-D segmentations should give a more precise measurement of the motion differences between rest and stress.

Although the protocol for selecting landmarks in the 3-D images was fixed, the intraobserver and interobserver variabilities were still large. This is inherently due to the poor image quality, but also due to the lack of a proper tool for viewing 3-D rest and stress images side-by-side. For this purpose, we are currently developing such a tool for analyzing 3-D rest-and-stress echocardiograms. With this software program, rest and stress data sets can be manually aligned using the protocol described in this study, and then visualized side-by-side and temporally synchronized. During initial tests, this tool proved to be a great help in the manual alignment, and has shown its use in improving the interobserver variability in wall motion analysis. The clinical evaluation of this tool is a subject of ongoing research.

Although this study is focused on spatial alignment, temporal alignment may further improve the comparison between rest and stress wall motion. The robust sparse registration setup would be very useful in this context, due to its low computation cost. The sparse planes can be annotated in ED and registered to the next time frame [30], [43], [68]. In this way, the landmarks can be propagated through the cardiac cycle automatically. Since the differences between two consecutive time-points are far smaller than between rest and stress, we anticipate that the registration can be performed more quickly and more accurately. A frame-to-frame registration within a single sequence should be a better alternative than registration of rest-stress images per time point, to avoid problems with temporal sampling (rest and stress sequences differ in number of time-points because the cardiac cycle is much shorter in stress). Investigation of the displacement of the manually annotated landmarks from ED to ES revealed that the motion of long-axis and the rotation of the four-chamber view are rather close to the interobserver variabilities. Therefore, it would be hard to show the improvement in alignment quantitatively in this study. Nevertheless, temporal registration may be useful to achieve more consistent views across the whole cardiac cycle.

### *G. Application*

We have demonstrated the effectiveness of sparse registration in echocardiograms, and we believe that it is also applicable to other registration problems. In any registration framework, it is important to emphasize the structures of which alignment is desired. This is especially true for images with many artifacts,

as we have shown in this study. Furthermore, by reducing the number of voxels with which the metric is calculated, the speed of registration can be greatly increased.

We are currently looking into fully automated methods for finding the sparse planes in the rest images. Recently, Liu and Yang described a template-matching based method to select the four-chamber view from 3-D echocardiograms [69]. We ourselves have experimented with active appearance model approaches [70]. Such methods will further facilitate wall motion comparison in stress echocardiography.

## V. Conclusion

In this study, sparse image registration was used for aligning rest and stress images for 3-D stress echocardiography. Orthogonal four-chamber, two-chamber, and short-axis planes of the 3-D rest image were registered to the 3-D stress image. Different configurations of planes were investigated. Registration using two long-axis planes and two short-axis planes was most successful, with a performance similar to manual alignment. In conclusion, sparse registration improves alignment of rest and stress images, making it an important step towards automated quantification in 3-D stress echocardiography.

## Acknowledgment

The authors would like to thank the sonographers of the Erasmus MC Thoraxcenter for acquiring the images. The authors also thank D. Alexander for advice in revising the manuscript.

## References

[1] T. H. Marwick, *Stress Echocardiography: Its Role in the Diagnosis and Evaluation of Coronary Artery Disease*, 2nd ed. Norwell, MA: Kluwer, 2003.

[2] W. F. Armstrong and W. A. Zoghbi, "Stress echocardiography: Current methodology and clinical applications," *J. Am. Coll. Cardiol.*, vol. 45, no. 11, pp. 1739–1747, Jun. 2005.

[3] H. S. Yang, P. A. Pellikka, R. B. McCully, J. K. Oh, J. A. Kukuzke, B. K. Khandheria, and K. Chandrasekaran, "Role of biplane and biplane echocardiographically guided 3-dimensional echocardiography during dobutamine stress echocardiography," *J. Am. Soc. Echocardiogr.*, vol. 19, no. 9, pp. 1136–1143, Sep. 2006.

[4] Y. Matsumura, T. Hozumi, K. Arai, K. Sugioka, K. Ujino, Y. Takemoto, H. Yamagishi, M. Yoshiyama, and J. Yoshikawa, "Non-invasive assessment of myocardial ischaemia using new real-time three-dimensional dobutamine stress echocardiography: Comparison with conventional two-dimensional methods," *Eur. Heart J.*, vol. 26, no. 16, pp. 1625–1632, Aug. 2005.

[5] D. R. Zwas, S. Takuma, S. Mullis-Jansson, A. Fard, H. Chaudhry, H. Wu, M. R. D. Tullio, and S. Homma, "Feasibility of real-time 3-dimensional treadmill stress echocardiography," *J. Am. Soc. Echocardiogr.*, vol. 12, no. 5, pp. 285–289, May 1999.

[6] C. Jenkins, J. Chan, L. Hanekom, and T. Marwick, "Accuracy and feasibility of online 3-Dimensional echocardiography for measurement of left ventricular parameters," *J. Am. Soc. Echocardiogr.*, vol. 19, no. 12, pp. 1119–1128, Sep. 2006.

[7] E. G. Caiani, C. Corsi, J. Zamorano, L. Sugeng, P. MacEneaney, L. Weinert, R. Battani, J. L. Gutierrez, R. Koch, L. P. de Isla, V. Mor-Avi, and R. M. Lang, "Improved semiautomated quantification of left ventricular volumes and ejection fraction using 3-dimensional echocardiography with a full matrix-array transducer: Comparison with magnetic resonance imaging," *J. Am. Soc. Echocardiogr.*, vol. 18, no. 8, pp. 779–788, Aug. 2005.

[8] M. Ahmad, T. Xie, M. McCulloch, G. Abreo, and M. Runge, "Real-time three-dimensional dobutamine stress echocardiography in assessment of ischemia: Comparison with two-dimensional dobutamine stress echocardiography," *J. Am. Coll. Cardiol.*, vol. 37, no. 5, pp. 1303–1309, Apr. 2001.

[9] R. Shekhar, V. Zagrodsky, M. J. Garcia, and J. D. Thomas, "Registration of real-time 3-D ultrasound images of the heart for novel 3-D stress echocardiography," *IEEE Trans. Med. Imag.*, vol. 23, no. 9, pp. 1141–1149, Sep. 2004.

[10] J. E. Pickard, S. T. Acton, and J. A. Hossack, "The effect of initialization and registration on the active shape segmentation of the myocardium in constrast enhanced ultrasound," in *Proc. IEEE Int. Ultrason. Symp.*, 2005, pp. 2066–2069.

[11] V. Zagrodsky, V. Walimbe, C. R. Castro-Pareja, J. X. Qin, J. M. Song, and R. Shekhar, "Registration-assisted segmentation of real-time 3-D echocardiographic data using deformable models," *IEEE Trans. Med. Imag.*, vol. 24, no. 9, pp. 1089–1099, Sep. 2005.

[12] V. Walimbe, V. Zagrodsky, and R. Shekhar, "Fully automatic segmentation of left ventricular myocardium in real-time three-dimensional echocardiography," *Proc. SPIE Med. Imag.*, vol. 6144, p. 61444H, 2006.

[13] D. L. G. Hill, P. G. Batchelor, M. H. Holden, and D. J. Hawkes, "Medical image registration," *Phys. Med. Biol.*, vol. 46, no. 3, pp. 1–45, Mar. 2001.

[14] J. B. A. Maintz and M. A. Viergever, "A survey of medical image registration," *Med. Image Anal.*, vol. 2, no. 1, pp. 1–36, Mar. 1998.

[15] J. P. Pluim, J. B. Maintz, and M. A. Viergever, "Mutual-information-based registration of medical images: A survey," *IEEE Trans. Med. Imag.*, vol. 22, no. 8, pp. 986–1004, Aug. 2003.

[16] T. Mäkelä, P. Clarysse, O. Sipilä, N. Pauna, Q. C. Pham, T. Katila, and I. E. Magnin, "A review of cardiac image registration methods," *IEEE Trans. Med. Imag.*, vol. 21, no. 9, pp. 1011–1021, Sep. 2002.

[17] J. P. W. Pluim and J. M. Fitzpatrick, "Image registration," *IEEE Trans. Med. Imag.*, vol. 22, no. 11, pp. 1341–1343, Nov. 2003.

[18] R. N. Rohling, A. H. Gee, and L. Berman, "Automatic registration of 3-D ultrasound images," *Ultrasound Med. Biol.*, vol. 24, no. 6, pp. 841–854, Jul. 1998.

[19] C. R. Meyer, J. L. Boes, B. Kim, P. H. Bland, G. L. Lecarpentier, J. B. Fowlkes, M. A. Roubidoux, and P. L. Carson, "Semiautomatic registration of volumetric ultrasound scans," *Ultrasound Med. Biol.*, vol. 25, no. 3, pp. 339–347, Mar. 1999.

[20] J. F. Krücker, C. R. Meyer, G. L. LeCarpentier, J. B. Fowlkes, and P. L. Carson, "3-D spatial compounding of ultrasound images using image-based nonrigid registration," *Ultrasound Med. Biol.*, vol. 26, no. 9, pp. 1475–1488, Sep. 2000.

[21] P. Foroughi and P. Abolmaesumi, "Intra-subject elastic registration of 3-D ultrasound images," *Med. Image Anal.*, vol. 10, no. 5, pp. 713–725, Oct. 2006.

[22] X. Pennec, P. Cachier, and N. Ayache, "Tracking brain deformations in time sequences of 3-D us images," *Pattern Recognit. Lett.*, vol. 24, no. 4–5, pp. 801–813, Feb. 2003.

[23] G. P. Penney, D. C. Barratt, C. S. K. Chan, M. Slomczykowski, T. J. Carter, P. J. Edwards, and D. J. Hawkes, "Cadaver validation of intensity-based ultrasound to CT registration," *Med. Image Anal.*, vol. 10, no. 3, pp. 385–395, Jan. 2006.

[24] G. P. Penney, J. M. Blackall, M. S. Hamady, T. Sabharwal, A. Adam, and D. J. Hawkes, "Registration of freehand 3-D ultrasound and magnetic resonance liver images," *Med. Image Anal.*, vol. 8, no. 1, pp. 81–91, Mar. 2004.

[25] A. Roche, X. Pennec, G. Malandain, and N. Ayache, "Rigid registration of 3-D ultrasound with MR images: A new approach combining intensity and gradient information," *IEEE Trans. Med. Imag.*, vol. 20, no. 10, pp. 1038–1049, Oct. 2001.

[26] M. M. J. Letteboer, P. W. A. Willems, M. A. Viergever, and W. J. Niessen, "Brain shift estimation in image-guided neurosurgery using 3-D ultrasound," *IEEE Trans. Biomed. Eng.*, vol. 52, no. 2, pp. 268–276, Feb. 2005.

[27] V. Grau and J. A. Noble, "Adaptive multiscale ultrasound compounding using phase information," *Proc. MICCAI 2005*, pp. 589–596, 2005.

[28] V. Grau, H. Becher, and J. A. Noble, "Phase-based registration of multi-view real-time three-dimensional echocardiographic sequences," *Proc. MICCAI 2006*, pp. 612–619, 2006.

[29] W. Zhang, J. A. Noble, and J. M. Brady, "Real time 3-D ultrasound to MR cardiovascular image registration using a phase-based approach," in *Proc. 3rd IEEE Int. Symp. Biomed. Imag.: Macro Nano*, 2006, pp. 666–669.

[30] M. J. Ledesma-Carbayo, J. Kybic, M. Desco, A. Santos, M. Sühling, P. Hunziker, and M. Unser, "Spatio-Temporal nonrigid registration for ultrasound cardiac motion estimation," *IEEE Trans. Med. Imag.*, vol. 24, no. 9, pp. 1113–1126, Sep. 2005.

[31] M. J. Ledesma-Carbayo, P. Mahía-Casado, A. Santos, E. Pérez-David, M. A. García-Fernández, and M. Desco, "Cardiac motion analysis from ultrasound sequences using nonrigid registration: Validation against doppler tissue velocity," *Ultrasound Med. Biol.*, vol. 32, no. 4, pp. 483–490, Apr. 2006.

[32] V. Walimbe, V. Zagrodsky, S. Raja, W. A. Jaber, F. P. DiFilippo, M. J. Garcia, R. C. Brunken, J. D. Thomas, and R. Shekhar, "Mutual information-based multimodality registration of cardiac ultrasound and SPECT images: A preliminary investigation," *Int. J. Cardiov. Imaging*, vol. 19, no. 6, pp. 483–494, Dec. 2003.

[33] J. Declerck, J. Feldmar, M. L. Goris, and F. Betting, "Automatic registration and alignment on a template of cardac stress and rest reoriented SPECT images," *IEEE Trans. Med. Imag.*, vol. 16, no. 6, pp. 727–737, Dec. 1997.

[34] T. Delzescaux, F. Frouin, A. de Cesare, S. Philipp-Foliguet, A. Todd-Pokropek, A. Herment, and M. Janier, "Using an adaptive semiautomated self-evaluated registration technique to analyze mri data for myocardial perfusion assessment," *J. Magn. Reson. Imag.*, vol. 18, pp. 681–690, 2003.

[35] P. J. Slomka, G. A. Hurwitz, J. Stephenson, and T. Cradduck, "Automated alignment and sizing of myocardial stress and rest scans to three-dimensional normal templates using an image registration algorithm," *J. Nucl. Med.*, vol. 36, pp. 1115–1122, 1995.

[36] P. J. Slomka, H. Nishina, D. S. Berman, X. Kang, J. D. Friedman, S. W. Hayes, U. E. Aladl, and G. Germano, "Automatic quantification of myocardial perfusion stress-rest change: A new measure of ischemia," *J. Nucl. Med.*, vol. 45, pp. 183–91, 2004.

[37] A. Juslin, J. Lotjonen, S. V. Nesterov, K. Kalliokoski, J. Knuuti, and U. Ruotsalainen, "Alignment of 3-dimensional cardiac structures in O-15-labeled water PET emission images with mutual information," *J. Nucl. Cardiol.*, vol. 14, pp. 82–91, 2007.

[38] R. Shekhar and V. Zagrodsky, "Mutual information-based rigid and non-rigid registration of ultrasound volumes," *IEEE Trans. Med. Imag.*, vol. 21, no. 1, pp. 9–22, Jan. 2002.

[39] B. Fei, J. L. Duerk, D. T. Boll, J. S. Lewin, and D. L. Wilson, "Slice-to-Volume registration and its potential application to interventional mri-guided radio-frequency thermal ablation of prostate cancer," *IEEE Trans. Med. Imag.*, vol. 22, no. 4, pp. 515–525, Apr. 2003.

[40] G. P. Penney, J. Weese, J. A. Little, P. Desmedt, D. L. G. Hill, and D. J. Hawkes, "A comparison of similarity measures for use in 2-D -3-D medical image registration," *IEEE Trans. Med. Imag.*, vol. 17, no. 4, pp. 586–595, Apr. 1998.

[41] M. D. Cerqueira, N. J. Weissman, V. Dilsizian, A. K. Jacobs, S. Kaul, W. K. Laskey, D. J. Pennell, J. A. Rumberger, T. Ryan, and M. Verani, "Standardized myocardial segmentation and nomenclature for tomographic imaging of the heart," *Circulation*, vol. 105, no. 3, pp. 539–542, Jan. 2002.

[42] B. P. F. Lelieveldt, R. J. van der Geest, H. J. Lamb, H. W. M. Kayser, and J. H. C. Reiber, "Automated observer-independent acquisition of cardiac short-axis MR images: A pilot study," *Radiology*, vol. 221, no. 2, pp. 537–542, Nov. 2001.

[43] F. Veronesi, C. Corsi, E. G. Caiani, A. Sarti, and C. Lamberti, "Tracking of left ventricular long axis from real-time three-dimensional echocardiography using optical flow techniques," *IEEE Trans. Inf. Technol. Biomed.*, vol. 10, no. 1, pp. 174–181, Jan. 2006.

[44] V. Mor-Avi, L. Sugeng, L. Weinert, P. MacEneaney, E. G. Caiani, R. Koch, I. S. Salgo, and R. M. Lang, "Fast measurement of left ventricular mass with real-time three-dimensional echocardiography, comparison with magnetic resonance imaging," *Circulation*, vol. 110, no. 13, pp. 1814–1818, Sep. 2004.

[45] D. Rueckert, L. I. Sonoda, C. Hayes, A. Hill, M. O. Leach, and D. J. Hawkes, "Nonrigid registration using free-form deformations: Applications to breast MR images," *IEEE Trans. Med. Imag.*, vol. 18, no. 8, pp. 712–721, Aug. 1999.

[46] K. McLeish, D. L. Hill, D. Atkinson, J. M. Blackall, and R. Razavi, "A study of the motion and deformation of the heart due to respiration," *IEEE Trans. Med. Imag.*, vol. 21, no. 9, pp. 1142–50, Sep. 2002.

[47] J. C. Lagarias, J. A. Reeds, M. H. Wright, and P. E. Wright, "Convergence properties of the Nelder-Mead simplex method in low dimensions," *SIAM J. Optim.*, vol. 9, no. 1, pp. 112–147, 1998.

[48] W. H. Press, S. A. Teukolsky, W. T. Vetterling, and B. P. Flannery, *Numerical Recipes in C—The art of Scientific Computing*, 2nd ed. Cambridge, U.K.: Cambridge Univ. Press, 1992.

[49] V. Zagrodsky, R. Shekhar, and J. F. Cornhill, "Multi-function extension of simplex optimization method for mutual information-based registration of ultrasound volumes," *Proc. SPIE Med. Imag. 2001: Image Process.*, vol. 4322, pp. 508–515, 2001.

[50] A. Giachetti, "Matching techniques to compute image motion," *Image Vis. Comput.*, vol. 18, no. 3, pp. 247–260, Feb. 2000.

[51] F. Maes, A. Collignon, D. Vandermeulen, G. Marchal, and P. Suetens, "Multimodality image registration by maximization of mutual information," *IEEE Trans. Med. Imag.*, vol. 16, no. 2, pp. 187–198, Apr. 1997.

[52] P. J. Burt and E. H. Adelson, "The laplacian pyramid as a compact image code," *IEEE Trans. Commun.*, vol. COM-31, no. 4, pp. 532–540, Apr. 1983.

[53] A. Nemes, M. L. Geleijnse, B. J. Krenning, O. I. I. Soliman, A. M. Anwar, W. B. Vletter, and F. J. T. Cate, "Usefulness of ultrasound contrast agent to improve image quality during real-time three-dimensional stress echocardiography," *Am. J. Cardiol.*, vol. 99, no. 2, pp. 275–278, Jan. 2007.

[54] M. M. Voormolen, B. J. Krenning, C. T. Lancee, F. J. ten Cate, J. R. T. C. Roelandt, A. F. W. van der Steen, and N. De Jong, "Harmonic 3-D echocardiography with a fast rotating ultrasound transducer," *IEEE Trans. Ultrason., Ferroelectr., Freq. Control*, vol. 53, pp. 1739–1748, 2006.

[55] D. G. Altman, *Practical statistics for medical research*, 1st ed. London, U.K.: Chapman Hall, 1997.

[56] Matlab—The language of technical computing. The MathWorks, Inc., Natick, MA, 2002.

[57] K. L. Chan, X. Liu, K. J. Ascah, L. M. Beauchesne, and I. G. Burwash, "Comparison of real-time 3-dimensional echocardiography with conventional 2-dimensional echocardiography in the assessment of structural heart disease," *J. Am. Soc. Echocardiogr.*, vol. 17, no. 9, pp. 976–80, Sep. 2004.

[58] H. C. van Assen, M. G. Danilouchkine, A. F. Frangi, S. Ordas, J. J. Westenberg, J. H. Reiber, and B. P. Lelieveldt, "SPASM: A 3D-ASM for segmentation of sparse and arbitrarily oriented cardiac mri data," *Med. Image Anal.*, vol. 10, no. 2, pp. 286–303, Apr. 2006.

[59] B. S. F. Pang, B. C. W. Kot, and M. Ying, "Three-dimensional ultrasound volumetric measurements: Is the largest number of image planes necessary for outlining the region-of-interest," *Ultrasound Med. Biol.*, vol. 32, no. 8, pp. 1193–1202, Aug. 2006.

[60] M. M. Voormolen, B. J. Krenning, R. J. M. Van Geuns, C. T. Lancée, W. B. Vletter, F. J. Ten Cate, J. R. T. C. Roelandt, A. F. W. Van der Steen, and N. De Jong, "Efficient quantification of the left ventricular volume using 3-Dimensional echocardiography: The minimal number of equiangular long-axis images for accurate quantification of the left ventricular volume," *J. Am. Soc. Echocardiogr.*, vol. 20, no. 4, pp. 373–380, Apr. 2007.

[61] F. A. Duck, "Nonlinear acoustics in diagnostic ultrasound," *Ultrasound Med. Biol.*, vol. 28, no. 1, pp. 1–18, Jan. 2002.

[62] B. Cohen and I. Dinstein, "New maximum likelihood motion estimation schemes for noisy ultrasound images," *Pattern Recognit.*, vol. 35, no. 2, pp. 455–463, Feb. 2002.

[63] C. R. M. Janssen, C. L. De Korte, M. S. Van der Heiden, C. P. A. Wapenaar, and A. F. W. Van der Steen, "Angle matching in intravascular elastography," *Ultrasonics*, vol. 38, pp. 417–423, Mar. 2000.

[64] K. Y. E. Leung, R. A. Baldewsing, F. Mastik, J. A. Schaar, A. Gisolf, and A. F. W. Van der Steen, "Motion compensation for intravascular ultrasound palpography," *IEEE Trans. Ultrason., Ferroelectr., Freq. Control*, vol. 53, no. 7, pp. 1269–1280, Jul. 2006.

[65] M. Otte, "Elastic registration of fMRI data using bézier-spline transformation," *IEEE Trans. Med. Imag.*, vol. 20, no. 2, pp. 193–206, Feb. 2001.

[66] B. Likar and F. Pernus, "A hierarchical approach to elastic registration based on mutual information," *Image Vis. Comput.*, vol. 19, pp. 33–44, 2001.

[67] J. Montagnat, M. Sermesant, H. Delingette, G. Malandain, and N. Ayache, "Anisotropic filtering for model-based segmentation of 4D cylindrical echocardiographic images," *Pattern Recognit. Lett.*, vol. 24, pp. 815–828, 2003.

[68] M. Sühling, M. Arigovindan, C. Jansen, P. Hunziker, and M. Unser, "Myocardial motion analysis from B-mode echocardiograms," *IEEE Trans. Image Process.*, vol. 14, no. 4, pp. 525–36, Apr. 2005.

[69] X. Liu and X. Yang, "Best cross-section auto-detection in 3-D echocardiac images," in *Proc. 1st Int. Workshop Comput. Vis. Intravascular Intracardiac Imag., MICCAI 2006*, 2006, pp. 107–114.

[70] K. Y. E. Leung, M. Van Stralen, G. Van Burken, M. M. Voormolen, A. Nemes, F. J. T. Cate, N. De Jong, A. F. W. Van der Steen, J. H. C. Reiber, and J. G. Bosch, "Sparse appearance model based registration of 3-D ultrasound images," *Proc. Med. Imag. Augmented Reality*, vol. 4091, pp. 236–243, 2006.